Published in final edited form as:
Neuroimage. 2013 December ; 83: . doi:10.1016/j.neuroimage.2013.06.047.

Direct Visualization of Short Transverse Relaxation Time Component (ViSTa)

Se-Hong Oh[1], **Michel Bilello**[1], **Matthew Schindler**[2], **Clyde E. Markowitz**[2], **John A. Detre**[1,2], and **Jongho Lee**[1]

[1]Department of Radiology, Perelman School of Medicine, University of Pennsylvania, Philadelphia, Pennsylvania, USA

[2]Department of Neurology, Perelman School of Medicine, University of Pennsylvania, Philadelphia, Pennsylvania, USA

Abstract

White matter of the brain has been demonstrated to have multiple relaxation components. Among them, the short transverse relaxation time component (T_2 < 40 ms; T_2^* < 25 ms at 3T) has been suggested to originate from myelin water whereas long transverse relaxation time components have been associated with axonal and/or interstitial water. In myelin water imaging, T_2 or T_2^* signal decay is measured to estimate myelin water fraction based on T_2 or T_2^* differences among the water components. This method has been demonstrated to be sensitive to demyelination in the brain but suffers from low SNR and image artifacts originating from ill-conditioned multi-exponential fitting. In this study, a novel approach that selectively acquires short transverse relaxation time signal is proposed. The method utilizes a double inversion RF pair to suppress a range of long T_1 signal. This suppression leaves short T_2^* signal, which has been suggested to have short T_1, as the primary source of the image. The experimental results confirms that after suppression of long T_1 signals, the image is dominated by short T_2^* in the range of myelin water, allowing us to directly visualize the short transverse relaxation time component in the brain. Compared to conventional myelin water imaging, this new method of direct visualization of short relaxation time component (ViSTa) provides high quality images. When applied to multiple sclerosis patients, chronic lesions show significantly reduced signal intensity in ViSTa images suggesting sensitivity to demyelination.

Keywords

background suppression; multiple water components in white matter; myelin water imaging; T_1 of myelin water; T_1 filter

Introduction

Myelin sheaths derived from oligodendrocytes provide electrical insulation surrounding axons to expedite signal conduction in the healthy brain. In certain inflammatory

Address correspondence to: Jongho Lee, 3 west Gates building, 3400 Spruce Street, Philadelphia, PA 19104, TEL: (215) 349-8462, jonghoyi@upenn.edu.

neurological disorders such as multiple sclerosis (MS), the myelin sheaths degenerate and cause disabilities. Failure of normal myelination also occurs in certain developmental disorders known as leukodystrophies. Restoration of oligodendrocytes and axonal myelination is a therapeutic target for both MS and leukodystriphies (Keough and Yong, 2013). Accordingly, the development of myelin or myelin-related biomarkers has important clinical implications for the diagnosis and prognosis of such diseases.

Several MRI methods including myelin water imaging (Mackay et al., 1994), magnetization transfer imaging (Balaban and Ceckler, 1992; Gass et al., 1994), and diffusion tensor imaging (Basser et al., 1994; Werring et al., 1999) have been proposed as potential biomarkers for myelin. Among them, myelin water imaging (MWI) measures signals from water molecules between neighboring myelin layers. It has been suggested that this fraction of water has shorter transverse relaxation time constants (T_2 and T_2^*) than other water inside of axons or in the extracellular space outside of fibers (Du et al., 2007b; Mackay et al., 1994; Menon and Allen, 1991; van Gelderen et al., 2012; Vasilescu et al., 1978). In a few studies, not only transverse relaxation but also longitudinal relaxation time constant (T_1) has been suggested to vary among the components (Deoni et al., 2008; Does and Gore, 2002; Helms and Hagberg, 2009; Koenig et al., 1990; Labadie et al., 2013; Lancaster et al., 2002; Stanisz et al., 2005). Similarly to the transverse relaxation time constants, the shortest T_1 component was assumed to have originated from myelin water.

In conventional MWI, the transverse relaxation is measured by multi-echo gradient echo (GRE) or spin echo (SE) sequences. Since the multiple water components have different relaxation times, the measured signal shows a multi-exponential decay. This decay is fitted with exponential decay basis functions to estimate the distribution of transverse relaxation time constants (Whittall and MacKay, 1989). Then the fraction of the short transverse relaxation time component or myelin water, which is approximately in the range of $T_2 < 40$ ms and $T_2^* < 25$ ms at 3 T (Hwang et al., 2010; Kolind et al., 2009; Oh et al., 2006), is calculated relative to the total water to generate a myelin water fraction (MWF) map. However, the fitting process is ill-conditioned and the resulting MWF map is sensitive to noise and artifacts (Cover, 2008; Reiter et al., 2009; Whittall and MacKay, 1989).

Here we propose a novel approach of selectively acquiring the short transverse relaxation time component in the brain. This method suppresses long T_1 signals such that the short T_1 signal dominates the image. We demonstrate that after long T_1 suppression, the remaining signals have T_2^* in the range of myelin water. The method is applied to MS patients and reveals that chronic lesions with demyelination have significant signal reduction compared to surrounding white matter. This new approach is referred to as direct Visualization of Short Transverse relaxation time component (ViSTa).

Methods

Double inversion RF pulses for long T_1 water suppression

An inversion recovery sequence using a single inversion RF pulse is commonly used to suppress a small range of T_1 signals. On the other hand, a pair of inversion RF pulse can be designed to suppress a wide range of T_1 (Duijn et al., 1992; Duyn et al., 2001). In this double inversion sequence, the transverse magnetization at an echo time (TE) after a 90° excitation can be written as follows:

$$M_{xy}=M_0\,(1-(2-(2-e^{-TD/T_1})e^{-TI_1/T_1})e^{-TI_2/T_1})e^{-TE/T_2^*} \quad \text{(Eq. 1)}$$

where the three intervals (TI_1, TI_2, and TD) are the time between the RF pulses as shown in Figure 1A. These intervals are adjusted to suppress the signal from the desired T_1 components.

In our method, the three intervals were chosen to have a large signal in short T_1 and a small signal in long T_1 such that the measured signal was dominated by the short T_1 component. Specifically, we optimized for the parameters that result in larger than 40% of fully relaxed magnetization (M_0) for $T_1 \leq 200$ ms (for a short T_1 component in white matter), 0.3 % or less for $750 \leq T_1 \leq 2000$ ms (for long T_1 components in white matter and gray matter), and 0.5% or less for 2000 ms $\leq T_1 \leq 5000$ ms (for CSF). The strict suppression of long T_1 components was, in part, because the T_1 of myelin water at 3 T is not well characterized (see Discussion). As a result, the sequence parameters were chosen to have minimal contribution from long T_1 signals while keeping a relatively large signal from the short T_1 component. To find the parameters that satisfy this condition, a parameter search was performed on TI_1, TI_2, and TD over the range of 10 ms to 1000 ms in the step size of 10 ms. The optimal inversion timing that satisfied the condition was TI_1 = 560 ms, TI_2 = 220 ms, and TD = 380 ms. The resulting transverse magnetization is shown in Figure 1B. These parameters suppress signals not only from long T_1 components in white matter (750 to 1000 ms at 3 T), but also from gray matter (1300 to 1800 ms at 3 T) and CSF (~ 4000 ms at 3 T). This suppression helps to avoid bright regions and artifacts in the image. Similarly, fat can be suppressed using a fat saturation pulse before the RF excitation at the cost of slight signal reduction from the magnetization transfer (MT) effect. Thus, all static signals except the short T_1 signal were suppressed. When these parameters are used, the signal from the short T_1 component may also be attenuated if T_1 is longer than 100 ms. Hence, the method may show sensitivity to both the fraction and T_1 of the short T_1 component.

To demonstrate that the suppression of long T_1 components resulted in short T_2^* signal in the range of myelin water, the double inversion sequence was acquired with multi-echo readout and the resulting signal decay curves were compared with those from conventional GRE. A MWF map was generated from the GRE data and compared to a ViSTa image.

All healthy volunteers and patients participated in the study provided written consent approved by an institutional review board.

MRI scans in healthy volunteers

Data were collected from 5 healthy subjects (mean age = 32 ± 3 years). A 3 T MRI scanner (Trio, Siemens, Erlangen, Germany) was used with a 32 channel head array receiver. The scan started with a localizer, followed by a region-of-interest shimming over the brain area. Three acquisitions were performed as follows:

Scan 1) A double inversion prepared multi-echo GRE sequence (ViSTa sequence): single slice, FOV = 220 mm^2, resolution = 1.38 × 1.38 mm^2, slice thickness = 3 mm, TR = 1160 ms, TI_1 = 560 ms, TI_2 = 220 ms, TD = 380 ms, TE = 1.95 ms to 84.1 ms (echo spacing = 2.65 ms), number of echoes = 32, flip angle = 90° (duration = 1 ms; sinc), matrix size = 160 × 160, bandwidth = 710 Hz/pixel, and scan time = 3.1 min. A non-selective hyperbolic secant pulse (duration = 10.24 ms and bandwidth = 1 kHz) was used for the inversion pulses. The sequence was repeated five times (15.5 min) and the images were averaged to improve SNR. No fat saturation was applied. In three subjects, additional data were acquired with fat saturation (no average) to estimate the signal reduction from the MT effect.

Scan 2) A multi-echo GRE sequence for GRE-MWI: An RF-spoiled GRE sequence with no double inversion RF pulses with the same scan parameters as Scan 1 except TR

(= 97 ms) and flip angle (= 28°). The data was collected 12 times and averaged. The total scan time was 3.1 min.

Scan 3) A ViSTa sequence using a single echo with a low readout bandwidth: the same sequence structure and parameters as in Scan 1 except number of echoes = 1, TE = 6.36 ms, and bandwidth = 100 Hz/pixel. The total scan time was 3.1 min (no average). A fat saturation pulse was applied to remove bright fat signal.

Data from Scan 1 and Scan 2 were used to compare signal characteristics of ViSTa and GRE. Data from Scan 2 and Scan 3 were used to compare the spatial distributions of short T_2^* and image quality between ViSTa and GRE.

Data analysis

To characterize the multi-component signal decays in the ViSTa (Scan 1) and GRE data (Scan 2), ROI analysis was performed at five manually drawn ROIs: genu, splenium, major forceps, minor forceps and internal capsule. In each ROI, a mean decay curve was generated by averaging signals within the ROI. The distribution of the multiple components was estimated by fitting the mean decay curve with multiple exponential T_2^* decays (Whittall and MacKay, 1989), given by:

$$y_i = \sum_{k=1}^{M} s_k \exp\left(-\frac{t_i}{T_{2k}^*}\right), \quad i = 1, 2, \ldots, N \quad \text{(Eq. 2)}$$

where t_i is an echo time, y_i is the measured decay at t_i, N is the total number of echoes, and s_k and T_{2k}^* are the relative amplitude and T_2^* for each component respectively. M (= 120) is the number of T_2^* decay components in the model. T_{2k}^* is spaced logarithmically from 2.77 ms to 300 ms (Lenz et al., 2011). To estimate the relative amplitude of each component, a nonnegative least-square (NNLS) fitting method, widely used in MWI, was applied (Whittall and MacKay, 1989). Regularization, which is to find s_k that minimizes $\chi^2 + \mu \sum_{k=1}^{M} s_k^2$ where μ is positive and χ^2 is a residual sum of squares with the constraint of $1.02\chi^2_{min} \leq \chi^2 \leq 1.025\chi^2_{min}$, was tested but was not applied in the ROI analysis because SNR was very high after ROI averaging (ROI-averaged first echo SNR was over 420) and the estimated myelin water fraction was very similar (7.2% vs. 7.0% in GRE and 95.4 % vs. 95.1% in ViSTa for non-regularized vs. regularization). The regularization was applied to generate a MWF map in GRE data where the NNLS fitting was performed in individual voxels.

In the ViSTa images, the signal level was low and, therefore, non-zero mean noise distribution of the magnitude images resulted in a constant offset in the decay curves (Henkelman, 1985). This offset biases the T_2^* estimation and, therefore, was subtracted from the data before the fitting process (Gambarota et al., 2001; Ghugre et al., 2005). The offset was estimated by averaging a background noise area outside of the head.

The NNLS fitting resulted in a distribution of T_2^* components. T_2^* components between 3 ms and 25 ms were regarded as myelin water (Hwang et al., 2010). The MWF was calculated as a ratio between sum of the myelin water components and sum of all components.

In the ViSTa data, the fraction of the short T_2^* signal relative to total water signal was estimated in each ROI. The signal intensity of the short T_2^* component at TE = 0 ms was extrapolated using the short T_2^* components (i.e. 3 ms < T_2^* < 25 ms) estimated in the NNLS fitting results in the ViSTa data. The total water signal was estimated from the GRE

data (Scan 2) by extrapolating the signal intensity at TE = 0 ms using all components in the NNLS fitting results. Since the measured GRE signal is total water signal multiplied by $(1 - e^{-TR/T1})\cdot\sin\theta/(1 - e^{-TR/T1}\cdot\cos\theta)$, the estimated signal intensity at TE = 0 ms was divided by 0.25 assuming T_1 to be 800 ms. The ratio of short T_2^* signal to total water signal at TE = 0 was then calculated and compared with the MWF of GRE-MWI. The same receiver gain was used for both ViSTa and GRE scans for this quantification.

In addition to the ROI analysis, the GRE data were processed using the regularized NNLS method in voxel-by-voxel basis to generate a MWF map. In the GRE-MWF map, the mean MWF in each ROI was calculated and compared with the MWF calculated in the ROI analysis.

The GRE-MWF map was compared with both a single-echo ViSTa image from Scan 3, and a normalized ViSTa image. The normalization of ViSTa was performed as follows: First, the single-echo ViSTa image was divided by the first echo GRE image. The resulting image was multiplied by a magnitude-thresholded mask generated from the GRE image to avoid noise amplification. Then, a scaling factor was multiplied to compensate for T_1- and T_2^*-weighting in GRE and ViSTa. This scaling factor was calculated using nominal T_1 and T_2^* values. In GRE, nominal T_1 and T_2^* were assumed to be 800 ms and 40 ms respectively. In ViSTa, nominal T_1 and T_2^* were 118 ms and 10 ms respectively and the signal was assumed to originate fully from the short T_2^* component. The resulting scaling factor was (GRE T_1-weight × GRE T_2^*-weight) / (ViSTa T_1-weight × ViSTa T_2^*-weight) = (0.25 × 0.95) / (0.69 × 0.53) = 0.65. Since the normalization was performed using nominal values, the resulting image has limited accuracy in quantification (see Discussion). In this study, the primary purpose of the normalization was to remove coil sensitivity from the ViSTa images so that the spatial distribution of short T_2^* signal in the brain can be compared between ViSTa and GRE-MWF.

MRI scans in multiple sclerosis patients

Images were acquired from clinically diagnosed MS patients to demonstrate signal characteristics of ViSTa in MS lesions. Four patients were scanned on a clinical 3T MRI scanner (Trio, Siemens) that was different from the scanner used for the healthy volunteers. A 12 channel phased-array head coil (Matrix, Siemens) was used for data acquisition. The ViSTa sequence was acquired in addition to a routine clinical MS protocol. The sequence was acquired after magnetization prepared rapid acquisition gradient echo (MPRAGE; sagittal orientation), flow-attenuated inversion recovery (FLAIR; axial orientation) and proton density-weighted (PDW; axial orientation) scans, prior to contrast administration. The resolutions were 1 × 1 × 1 mm^3 for MPRAGE, 0.86 × 0.86 × 3 mm^3 for FLAIR, and 0.34 × 0.34 × 3 mm^3 for PDW. A single slice that clearly contained lesions in FLAIR and PDW images was chosen as the imaging slice for the ViSTa scan. A post-contrast MPRAGE data was acquired following contrast agent injection (Gd-DTPA). ViSTa scan was acquired with slightly different scan parameters in each patient. In Patient 4 (shown in Figure 5), the parameters were as follows: resolution = 1.38 × 1.38 mm^2, number of echoes = 1 echo, TE = 6.12 ms, flip angle for excitation = 90°, slice thickness = 3 mm, and scan time = 3.1 min. The same double inversion RF timing used in the healthy volunteer scans was applied. Data were acquired three times to improve SNR. A GRE scan of matching parameters with 32 echoes was also acquired but data showed in poor quality MWI, most likely due to poor shim.

Results

The images acquired with GRE and ViSTa are shown in Figure 2. The display scale is different between the two scans and the maximum range of the first echo image was twice

that of the other echo images. The GRE images show significant signal drop in the frontal lobe area at the last echo due to field inhomogeneity (Fig. 2C). The first echo ViSTa image reveals that white matter has high signal intensity whereas gray matter areas show substantially reduced signal (Fig. 2D). CSF also shows substantial signal reduction but has residual signal potentially originating from CSF flow (Stadlbauer et al., 2010). Arteries and fat are also highlighted in the ViSTa images because of inflow of blood and short T_1 of fat. In the last echo (Fig. 2F), white matter signal reaches the noise level.

The measured signal decays and T_2^* distributions in each ROI are shown in Figure 3 (genu – blue, splenium – red, major forceps – green, minor forceps – cyan, and internal capsule – magenta). Compared to the decay curves from the GRE scan (Fig. 3A), the ViSTa signals decay much more rapidly (Fig. 3C). This is also clearly demonstrated in the T_2^* distribution from the NNLS fitting (Fig. 3B *vs.* 3D) confirming that the primary ViSTa signal has shorter T_2^* than the GRE signals. The T_2^* distributions from the GRE data (Fig. 3B) show a small fraction of the short T_2^* component (7.2 ± 1.2 %; an average of all subjects in splenium, major forceps and internal capsule ROIs hereafter unless noted) similar to a recent study (Lenz et al., 2011). In contrast, the ViSTa results demonstrate that the primary signals are from the short T_2^* component (95.4 ± 4.1 %) in the range of myelin water (3 ms < T_2^* < 25 ms). These results confirm that the suppression of long T_1 primarily leaves short T_2^* signal in the range of myelin water.

Compared to other ROIs, the signals from genu and minor forceps decay faster in the GRE data (Figs. 3A). This rapid T_2^* decay is from the field inhomogeneity effects where intravoxel dephasing induces additional signal loss. As a result, the T_2^* distributions show relatively shorter T_2^* with no myelin water peak (Fig. 3B). This has been observed in the previous studies (Hwang and Du, 2009; Hwang et al., 2010). In a few subjects, the primary T_2^* peak became less than 25 ms miscategorizing the signal as myelin water. Since this decay does not reflect intrinsic T_2^* decay of white matter, the genu and minor forceps were excluded from the ROI averages (Table 1). In the ViSTa data, on the other hand, expedited decay is not clearly observed in the two ROIs, however, in a few subjects, the decay resulted in two short T_2^* peaks (both within 25 ms). This may reflect spatially varying field inhomogeneity effects across an ROI and/or inflow artifact from neighboring vessels. The signal fractions of these ROIs are similar to the other ROIs and listed in Table 1. However, they are excluded from the ROI averages for a comparison with GRE data.

When the fraction of short T_2^* signal in ViSTa relative to total water signal was calculated, the results yielded on average 5.5 ± 0.4 % (the same result were obtained when averaged over splenium, major forceps, and internal capsule ROIs and when averaged over all ROIs; Table 1). This suggests that overall the short T_2^* signal fraction in ViSTa is slightly smaller than the myelin water fraction measured in the GRE data (7.2 % ± 1.2 % when signals were averaged over an ROI first and estimated and 7.5 ± 1.6 % when MWF values were averaged over ROIs from a MWF map; Table 1) (see Discussion).

In Figure 4, the MWF maps from the GRE data are compared to the original and normalized ViSTa images from Scan 3 (the same 3.1 min. scan). Both GRE-MWF and normalized ViSTa images reveal higher intensity in splenium, internal capsule and optic radiation areas than neighboring white matter. The GRE-MWF images (Figs. 4A and 4D) show either no MWF or excessive MWF in the frontal lobe area due to the field inhomogeneity which has been reported in previous studies (Hwang et al., 2011; Hwang et al., 2010). When comparing remaining brain areas, the ViSTa images still show superior image quality with much less speckle artifact. This is also true when comparing the ViSTa images to SE-based MWI in the literature (Kolind et al., 2009). Compared to the conventional MWI, ViSTa has limited accuracy in quantification due to T_1-weighting and other factors (see Discussion for

apparent MWF in ViSTa). Despite this limitation, ViSTa may provide clinically useful information in detecting demyelination (Figure 5).

Figure 5 shows FLAIR, PDW, post-contrast MPRAGE, and ViSTa images from an MS patient (Patient 4). The two large lesions (arrows) did not show signal enhancement in the post-contrast MPRAGE image (Fig. 5C) suggesting they are, so-called, T_1 black holes with demyelination and axonal loss. In these lesions, the ViSTa image shows significantly reduced signal levels successfully delineating the lesions (Fig. 5D). Venous in-flow is noticeable in the ViSTa image. The other three patients also showed T_1 black hole lesions and the corresponding areas in ViSTa had signal reduction (see supplementary figure for additional patient data).

When the effect of fat saturation was evaluated by comparing the first echo signal intensity with and without fat saturation, the signal dropped by 12.5% (three subjects, averaged over all ROIs). This may originate from the magnetization transfer effects. Fat saturation improves the visualization of the short T_2^* signal by suppressing bright fat signal (Fig. 2D vs. Fig. 4B) but is optional and can be removed for better quantification.

Discussion

In this work, a new method that selectively acquires short T_2^* signal by suppressing long T_1 signal is demonstrated. The experimental results show that the remaining signal is dominated by the short T_2^* signal (on average, 95.4%), confirming that the suppression of long T_1 leaves primarily short T_2^* signal. This observation can be explained by a multiple water component model in white matter that includes a short T_1 and T_2^* component and long T_1 and T_2^* component(s) (Deoni et al., 2008; Does and Gore, 2002; Helms and Hagberg, 2009; Koenig et al., 1990; Labadie et al., 2013; Lancaster et al., 2002; Stanisz et al., 2005). The observed signal decay after the long T_1 suppression shows T_2^* values in the range of myelin water indicating that the remaining signal is from myelin water. The fraction of the short T_2^* signal over total water signal (on average 5.5 ± 0.4%) in ViSTa is in a similar range to the myelin water fraction in GRE-MWI (7.2 ± 1.2%), though the slightly reduced fraction suggests that there may be additional T_1-weighted signal loss from the double inversion. The patient data further support the origin of ViSTa signal as myelin water. In the MS lesions, the FLAIR, PDW, and MPRAGE images suggest that the average water signal, dominated by long T_1 components, has increased T_1, T_2, and proton density signal compared to surrounding white matter. However, the signal in the ViSTa image was decreased. This cannot be explained by the changes in the long T_1 components because increases in proton density and T_2 of the long T_1 components would cause an increase in ViSTa signal. The increase in T_1 in long T_1 components may reduce the signal depending on the T_1 value. However, the measured signal relative to total water (5.5%) is substantially larger than the expected signal in the range of $T_1 > 750$ ms (0.5% or less). Hence, the changes in the long T_1 components alone cannot explain the signal reduction in MS lesions. On the other hand, these lesions are expected to have severe demyelination that will result in signal reduction in ViSTa due to the loss of myelin water. Hence, our data support a multiple water component model that has a short T_1 and T_2^* component and long T_1 and T_2^* components. More importantly, T_2^* characteristics and MS patient results suggest that the short T_2^* signal in ViSTa is from myelin water.

In the ViSTa sequence, the T_1 relaxation of the short T_2^* component (or myelin water) is an important design parameter for sequence optimization. However, measuring the actual T_1 is challenging due to the small fraction (~ 10%) and the short relaxation time ($T_2^* < 25$ ms at 3 T). Previous studies have suggested that myelin water has shorter T_1 than that of the other water components (Deoni et al., 2008; Does and Gore, 2002; Helms and Hagberg, 2009;

Koenig et al., 1990; Labadie et al., 2013; Lancaster et al., 2002; Stanisz et al., 2005). The estimated value ranges from 118 ms at 3 T (Labadie et al., 2013) to at 390 ms at 1.5 T (Deoni et al., 2008). Some of these values were estimated using multi-parametric fitting, which is known to be sensitive to a model under investigation (e.g. two pool vs. three pool), initial values, and search ranges. Recently, Labadie et al., used T_1 relaxography and suggested T_1 of myelin water as 118 ms (the median value of all measurements) at 3 T (Labadie et al., 2013). At this T_1 value, the myelin water signal in ViSTa will have 69% of the fully relaxed myelin water signal (Eq. 1) and ViSTa signal will have a myelin water fraction of 5.0% relative to total water signal which is calculated as the multiplication of the mean MWF (7.2%) in GRE-MWI and the signal reduction factor (0.69). This estimation is very close to our measurement in ViSTa (5.5%). Further research is necessary to accurately estimate the T_1 of myelin water value. Once the T_1 is known, a better sequence timing can be designed to improve SNR and quantification in ViSTa.

Other potential origins of the smaller short T_2^* fraction observed in ViSTa are cross-relaxation and chemical exchange between myelin water and macromolecules. Alternatively, a relatively short TR (= 97 ms) used for GRE may have increased myelin water fraction in GRE-MWI (Du et al., 2007b). Further research is necessary for a complete understanding of ViSTa signal.

Because of the confounding factors such as T_1-weighting and exchange, ViSTa may have limited accuracy in quantifying myelin water fraction. Furthermore, the single-echo ViSTa acquisition used a relatively long TE (= 6.36 ms), and the resulting T_2^*-weighting was corrected by nominal T_2^*. This nominal correction can be an additional source of error in quantification. When the estimated fractions were compared between multi-echo ViSTa results and single-echo ViSTa results (all subjects and all ROIs), the difference was relatively small (mean fraction was 5.5 % in multi-echo data, and 6.0 % in single-echo data). This error can be further reduced by using a spiral or radial sequence with a short TE (< 1 ms). Because of these confounding factors, the fraction measured in our experiment may be referred to as apparent myelin water fraction (aMWF) to distinguish it from conventional MWF. Despite this limitation, ViSTa can provide qualitative myelin water images with no post-processing, and generate high quality images with demonstrated sensitivity to MS lesions. These features make ViSTa appealing for clinical applications where myelination is being assessed. Note that conventional MWF has also been reported to be sensitive to field strength, coil, parameters in sequence and post-processing (Guo et al., 2012; Kolind et al., 2009).

In the original ViSTa images (Figs. 4B and 4E), no post-processing was performed and the images have coil sensitivity weighting. This can be removed using a coil sensitivity map or a proton density image. In our data (Figs. 4C and 4F), the correction was performed by dividing the first echo GRE images that has slight T_1-weighting. This weighting resulted in unwanted CSF enhancement in Figs 4C and 4F (arrows). The CSF enhancement can be removed by using a small flip angle (~ 5°) in GRE.

Conventional myelin water imaging has been shown to provide good sensitivity to demyelination (Laule et al., 2008; Laule et al., 2004; Mackay et al., 1994). It has also been suggested to differentiate demyelination from inflammation or edema, which is challenging with conventional MRI (Laule et al., 2007; Stanisz et al., 2004). Thus, MWI may have important diagnostic value in differentiating inflammatory lesions with and without demyelination. ViSTa may share the same advantage because inflammation, which is characterized by increased extracellular volume fraction, has been shown to produce limited changes in myelin water fraction and myelin water T_2 distribution (Stanisz et al., 2004). Inflammation induced myelin water T_1 change has not yet been studied and needs further

investigation. If confirmed, the high image quality of ViSTa will be advantageous in detecting demyelinated lesions and distinguishing them from other types of lesions.

In our study, ViSTa was compared to GRE-MWI. The GRE- MWI requires less SAR and provides larger volume coverage than SE- MWI. However, the GRE-based method suffers from sensitivity to B_0 field inhomogeneity (e.g. frontal lobe area in Fig. 4A). Techniques have been proposed to compensate for the field inhomogeneity effects (Hwang and Du, 2009; Hwang et al., 2010). Unlike GRE-based MWI, ViSTa does not require multiple echoes and generates myelin water images even near regions of field inhomogeneity.

The future extension of ViSTa for 3D coverage can be achieved by replacing the 2D single-echo ViSTa readout to a 3D multi-shot EPI, 3D interleaved stack-of-spiral, or 3D radial readout. Radial and spiral trajectories have the additional advantage of acquiring the center of k-space prior to T_2^* decay and, therefore, may provide higher SNR and improved quantification.

In a few studies, an inversion RF pulse prepared ultra-short echo time acquisition sequence (IR-UTE) was suggested to acquire short T_2^* signals in white matter (Du et al., 2007a; Waldman et al., 2003; Wilhelm et al., 2012). The inversion time was optimized to suppress long T_1 signals in white matter. Additionally, two echoes ($TE_1 = 8 \sim 80$ μs; $TE_2 = 1.2 \sim 11.08$ ms) were acquired to further reduce long T_2^* signal contribution by subtracting the second echo from the first echo. Recently, Wilhelm et al. (Wilhelm et al., 2012) have demonstrated that when the duration of RF (~ 20 μs) and TE_2 (= 1.2 ms) are short, the signal originates primarily from myelin protons ($T_2^* < 1$ ms) that exist inside the myelin and are different from myelin water protons. On the other hand, ViSTa uses a relatively long RF (1 ms) and TE (1.95 ~ 6.36 ms) and, therefore, has limited contribution from myelin proton signal.

Recently, several other new approaches that utilize magnetic susceptibility characteristics of myelin have been proposed to assess the integrity of myelin (Cohen-Adad et al., 2012; Duyn et al., 2007; Lee et al., 2010; Lee et al., 2011; Li et al., 2012; Liu, 2010; Miller et al., 2010; Wilhelm et al., 2012). These approaches, in conjunction with diffusion and MT imaging, may provide complementary information to ViSTa. The combination of these modalities may help us to better understand the biophysics of white matter and provide clinically useful information.

Conclusions

In this paper, we proposed a new approach to directly acquire short T_2^* signal. The method utilizes a double inversion RF scheme to suppress long T_1 water signals. After the suppression, a short T_2^* component in the range of myelin water dominated the image. The method provides high quality images and successfully detected MS demyelinated lesions.

Supplementary Material

Refer to Web version on PubMed Central for supplementary material.

Acknowledgments

This work was supported by NIH EB015893 and a Penn Medicine Comprehensive Neuroscience Center Pilot Grant.

References

Balaban RS, Ceckler TL. Magnetization transfer contrast in magnetic resonance imaging. Magn Reson Q. 1992; 8:116–137. [PubMed: 1622774]

Basser PJ, Mattiello J, LeBihan D. MR diffusion tensor spectroscopy and imaging. Biophys J. 1994; 66:259–267. [PubMed: 8130344]

Cohen-Adad J, Polimeni J, Helmer K, Benner T, McNab J, Wald L, Rosen B, Mainero C. T2* mapping and B0 orientation-dependence at 7T reveal cyto- and myeloarchitecture organization of the human cortex. NeuroImage. 2012; 60:1006–1014. [PubMed: 22270354]

Cover KS. A robust and reliable method for detecting signals of interest in multiexponential decays. Rev Sci Instrum. 2008; 79:055106.1–055106.11. [PubMed: 18513091]

Deoni SCL, Rutt BK, Arun T, Pierpaoli C, Jones DK. Gleaning multicomponent T1 and T2 information from steady-state imaging data. Magn Reson Med. 2008; 60:1372–1387. [PubMed: 19025904]

Does MD, Gore JC. Compartmental study of T1 and T2 in rat brain and trigeminal nerve in vivo. Magn Reson Med. 2002; 47:274–283. [PubMed: 11810670]

Du, J.; Bydder, M.; T, AM.; Shimakawa, A.; Hinks, S.; Bydder, GM. Ultrashort TE (UTE) imaging and T2 quantification of short T2 components in brain white matter. Proceedings of the 15th Annual Meeting of ISMRM; Berlin, Germany. 2007a. p. 3368

Du YP, Chu R, Hwang D, Brown MS, Kleinschmidt-DeMasters BK, Singel D, Simon JH. Fast multislice mapping of the myelin water fraction using multicompartment analysis of T2* decay at 3T: a preliminary postmortem study. Magn Reson Med. 2007b; 58:865–870. [PubMed: 17969125]

Duijn J, Matson G, Maudsley A, Hugg J, Weiner M. Human brain infarction: proton MR spectroscopy. Radiology. 1992; 183:711–718. [PubMed: 1584925]

Duyn JH, Tan CX, Gelderen P, Yongbi MN. High-sensitivity single-shot perfusion-weighted fMRI†. Magn Reson Med. 2001; 46:88–94. [PubMed: 11443714]

Duyn JH, van Gelderen P, Li TQ, de Zwart JA, Koretsky AP, Fukunaga M. High-field MRI of brain cortical substructure based on signal phase. Proc Natl Acad Sci USA. 2007; 104:11796–11801. [PubMed: 17586684]

Gambarota G, Cairns BE, Berde CB, Mulkern RV. Osmotic effects on the T2 relaxation decay of in vivo muscle. Magn Reson Med. 2001; 46:592–599. [PubMed: 11550254]

Gass A, Barker G, Kidd D, Thorpe J, MacManus D, Brennan A, Tofts P, Thompson A, McDonald W, Miller D. Correlation of magnetization transfer ration with clinical disability in multiple sclerosis. Ann Neurol. 1994; 36:62–67. [PubMed: 8024264]

Ghugre NR, Enriquez CM, Coates TD, Nelson MD, Wood JC. Improved R2* measurements in myocardial iron overload. J Magn Reson Imag. 2005; 23:9–16.

Guo J, Ji Q, Reddick WE. Multi-slice myelin water imaging for practical clinical applications at 3.0 T. Magn Reson Med. 2012 available online.

Helms G, Hagberg GE. In vivo quantification of the bound pool T1 in human white matter using the binary spin bath model of progressive magnetization transfer saturation. Phys Med Biol. 2009; 54:N529–N540. [PubMed: 19904029]

Henkelman RM. Measurement of signal intensities in the presence of noise in MR images. Med Phys. 1985; 12:232–233. [PubMed: 4000083]

Hwang D, Chung H, Nam Y, Du YP, Jang U. Robust mapping of the myelin water fraction in the presence of noise: Synergic combination of anisotropic diffusion filter and spatially regularized nonnegative least squares algorithm. J Magn Reson Imag. 2011; 34:189–195.

Hwang D, Du YP. Improved myelin water quantification using spatially regularized non-negative least squares algorithm. J Magn Reson Imag. 2009; 30:203–208.

Hwang D, Kim D, Du Y. In vivo multi-slice mapping of myelin water content using T2* decay. NeuroImage. 2010; 52:198–204. [PubMed: 20398770]

Keough MB, Yong VW. Remyelination therapy for multiple sclerosis. Neurotherapeutics. 2013; 10:44–54. [PubMed: 23070731]

Koenig SH, Brown RD 3rd, Spiller M, Lundbom N. Relaxometry of brain: why white matter appears bright in MRI. Magn Reson Med. 1990; 14:482–495. [PubMed: 2355830]

Kolind SH, Mädler B, Fischer S, Li DKB, MacKay AL. Myelin water imaging: implementation and development at 3.0 T and comparison to 1.5 T measurements. Magn Reson Med. 2009; 62:106–115. [PubMed: 19353659]

Labadie C, Lee J-H, Rooney WD, Jarchow S, Aubert-Frécon M, Springer CS, Möller HE. Myelin water mapping by spatially regularized longitudinal relaxographic imaging at high magnetic fields. Magnetic Resonance in Medicine. 2013

Lancaster JL, Andrews T, Hardies LJ, Dodd S, Fox PT. Three-pool model of white matter. J Magn Reson Imaging. 2002; 17:1–10. [PubMed: 12500269]

Laule C, Kozlowski P, Leung E, Li DKB, MacKay AL, Moore G. Myelin water imaging of multiple sclerosis at 7 T: correlations with histopathology. NeuroImage. 2008; 40:1575–1580. [PubMed: 18321730]

Laule C, Vavasour I, Moore G, Oger J, Li D, Paty D, MacKay A. Water content and myelin water fraction in multiple sclerosis. J Neurol. 2004; 251:284–293. [PubMed: 15015007]

Laule C, Vavasour IM, Kolind SH, Li DKB, Traboulsee TL, Moore G, MacKay AL. Magnetic resonance imaging of myelin. Neurotherapeutics. 2007; 4:460–484. [PubMed: 17599712]

Lee J, Shmueli K, Fukunaga M, van Gelderen P, Merkle H, Silva AC, Duyn JH. Sensitivity of MRI resonance frequency to the orientation of brain tissue microstructure. Proc Natl Acad Sci U S A. 2010; 107:5130–5135. [PubMed: 20202922]

Lee J, van Gelderen P, Kuo L, Merkle H, Silva AC, Duyn JH. T2*-based fiber orientation mapping. NeuroImage. 2011; 57:225–234. [PubMed: 21549203]

Lenz C, Klarhöfer M, Scheffler K. Feasibility of in vivo myelin water imaging using 3D multigradient-echo pulse sequences. Magn Reson Med. 2011; 68:523–528. [PubMed: 22213038]

Li X, Vikram DS, Lim IAL, Jones CK, Farrell JAD, van Zijl P. Mapping Magnetic Susceptibility Anisotropies of White Matter in vivo in the Human Brain at 7 Tesla. NeuroImage. 2012; 62:314–330. [PubMed: 22561358]

Liu C. Susceptibility tensor imaging. Magn Reson Med. 2010; 63:1471–1477. [PubMed: 20512849]

Mackay A, Whittall K, Adler J, Li D, Paty D, Graeb D. In vivo visualization of myelin water in brain by magnetic resonance. Magn Reson Med. 1994; 31:673–677. [PubMed: 8057820]

Menon R, Allen P. Application of continuous relaxation time distributions to the fitting of data from model systmes and excised tissue. Magn Reson Med. 1991; 20:214–227. [PubMed: 1775048]

Miller KL, Smith SM, Jezzard P. Asymmetries of the balanced SSFP profile. Part II: White matter. Magn Reson Med. 2010; 63:396–406. [PubMed: 20099329]

Oh J, Han ET, Pelletier D, Nelson SJ. Measurement of in vivo multi-component T2 relaxation times for brain tissue using multi-slice T2 prep at 1.5 and 3 T. Magn Reson Imaging. 2006; 24:33–43. [PubMed: 16410176]

Reiter DA, Lin P-C, Fishbein KW, Spencer RG. Multicomponent T2 relaxation analysis in cartilage. Magn Reson Med. 2009; 61:803–809. [PubMed: 19189393]

Stadlbauer A, Salomonowitz E, van der Riet W, Buchfelder M, Ganslandt O. Insight into the patterns of cerebrospinal fluid flow in the human ventricular system using MR velocity mapping. NeuroImage. 2010; 51:42–52. [PubMed: 20152907]

Stanisz GJ, Odrobina EE, Pun J, Escaravage M, Graham SJ, Bronskill MJ, Henkelman RM. T1, T2 relaxation and magnetization transfer in tissue at 3T. Magn Reson Med. 2005; 54:507–512. [PubMed: 16086319]

Stanisz GJ, Webb S, Munro CA, Pun T, Midha R. MR properties of excised neural tissue following experimentally induced inflammation. Magnetic Resonance in Medicine. 2004; 51:473–479. [PubMed: 15004787]

van Gelderen P, de Zwart JA, Lee J, Sati P, Reich DS, Duyn JH. Nonexponential T2* decay in white matter. Magn Reson Med. 2012; 67:110–117. [PubMed: 21630352]

Vasilescu V, Katona E, Simplaceanu V, Demco D. Water compartments in the myelinated nerve. III. Pulsed NMR result. Experientia. 1978; 34:1443–1444. [PubMed: 309823]

Waldman A, Rees JH, Brock CS, Robson MD, Gatehouse PD, Bydder GM. MRI of the brain with ultra-short echo-time pulse sequences. Neuroradiology. 2003; 45:887–892. [PubMed: 14508620]

Werring DJ, Clark CA, Barker GJ, Thompson AJ, Miller DH. Diffusion tensor imaging of lesions and normal-appearing white matter in multiple sclerosis. Neurology. 1999; 52:1626–1626. [PubMed: 10331689]

Whittall KP, MacKay AL. Quantitative interpretation of NMR relaxation data. JMR. 1989; 84:134–152.

Wilhelm MJ, Ong HH, Wehrli SL, Li C, Tsai PH, Hackney DB, Wehrli FW. Direct magnetic resonance detection of myelin and prospects for quantitative imaging of myelin density. PNAS. 2012; 109:9605–9610. [PubMed: 22628562]

Highlights

- A new approach that selectively acquire short T^{2*} is demonstrated.
- Signal characteristics suggest that the primary signal is from myelin water.
- MS lesions show signal reduction demonstrating sensitivity to demyelination.

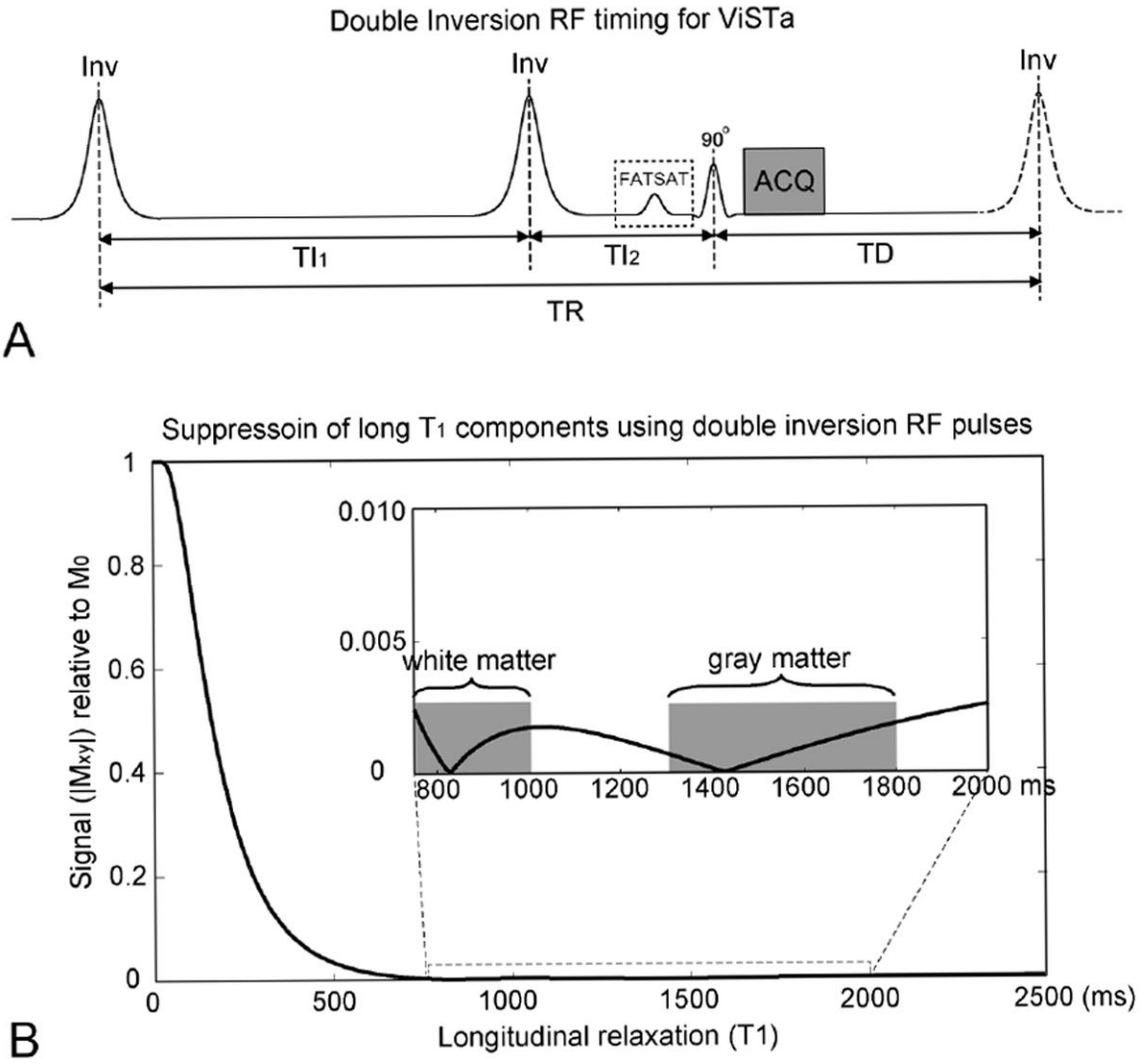

Figure 1.

(A) Double inversion RF pulse sequence for direct visualization of short transverse relaxation time component imaging (ViSTa). The timing (TI_1 = 560 ms, TI_2 = 220 ms, and TD = 380 ms) was optimized to have maximum suppression in water signal in the range of $750 \leq T_1 \leq 5000$ ms. (B) Transverse magnetization as a function of T_1 in the ViSTa sequence. The double inversion pulse enabled signal suppression over a wide range of long T_1.

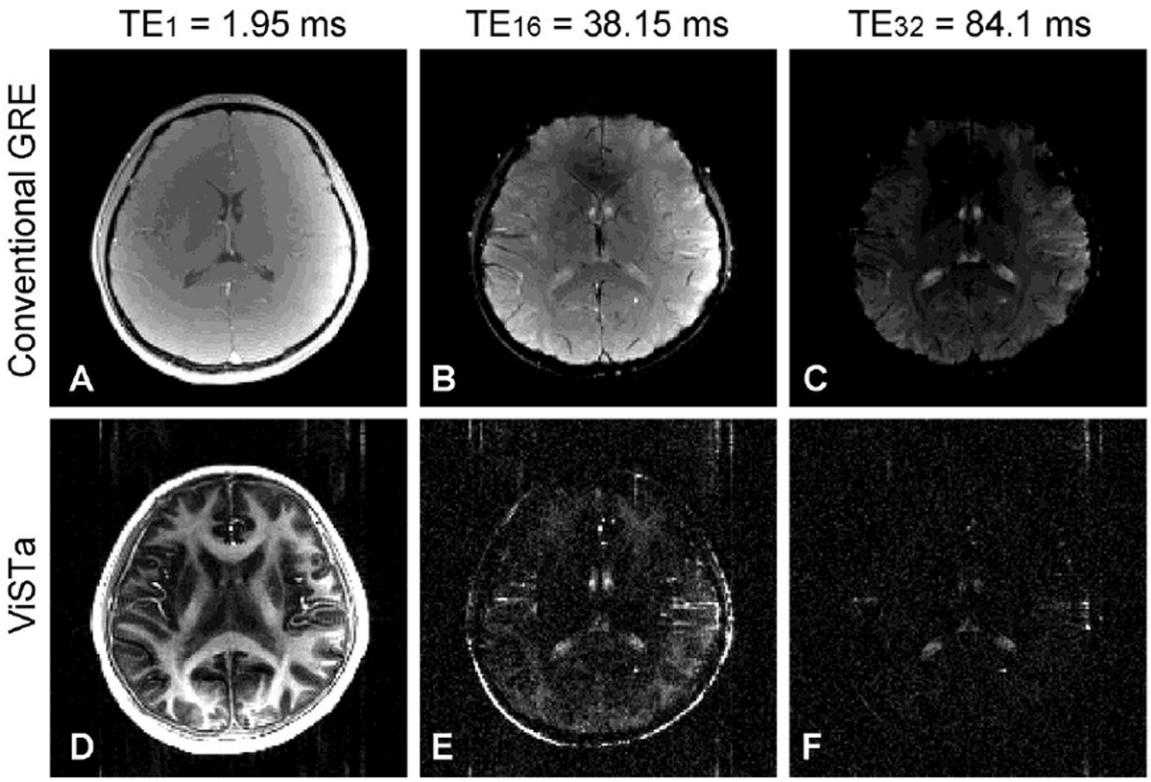

Figure 2.
(A) – (C) The first, 16th and last echo images from GRE. (D) – (F) The same three echo images from ViSTa. Flow artifacts in the phase encoding direction (anterior-posterior) is observed in the ViSTa images.

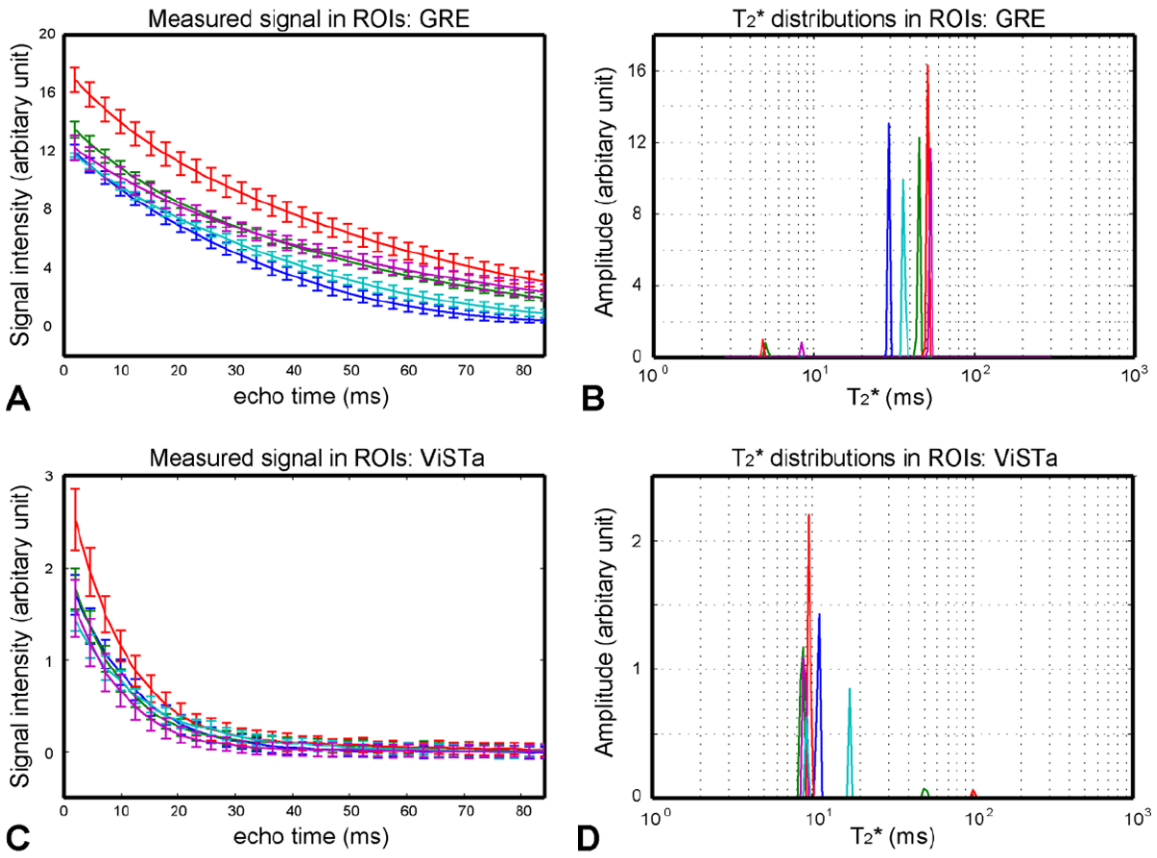

Figure 3.

Signal decay measurements in GRE (A) and ViSTa (C). NNLS multi-exponential fitted results in GRE (B) and ViSTa (D). The lines are color coded as follows: Genu – blue, splenium – red, major forceps – green, minor forceps – cyan, and internal capsule – magenta. The signals in ViSTa decay much rapidly compared to those in GRE. The resulting T_2^* distributions (D) suggest that the primary component in ViSTA has T_2^* less than 25 ms. On the other hand, the GRE results (C) show the signal dominance from a long T_2^* component ($T_2^* > 25$ ms).

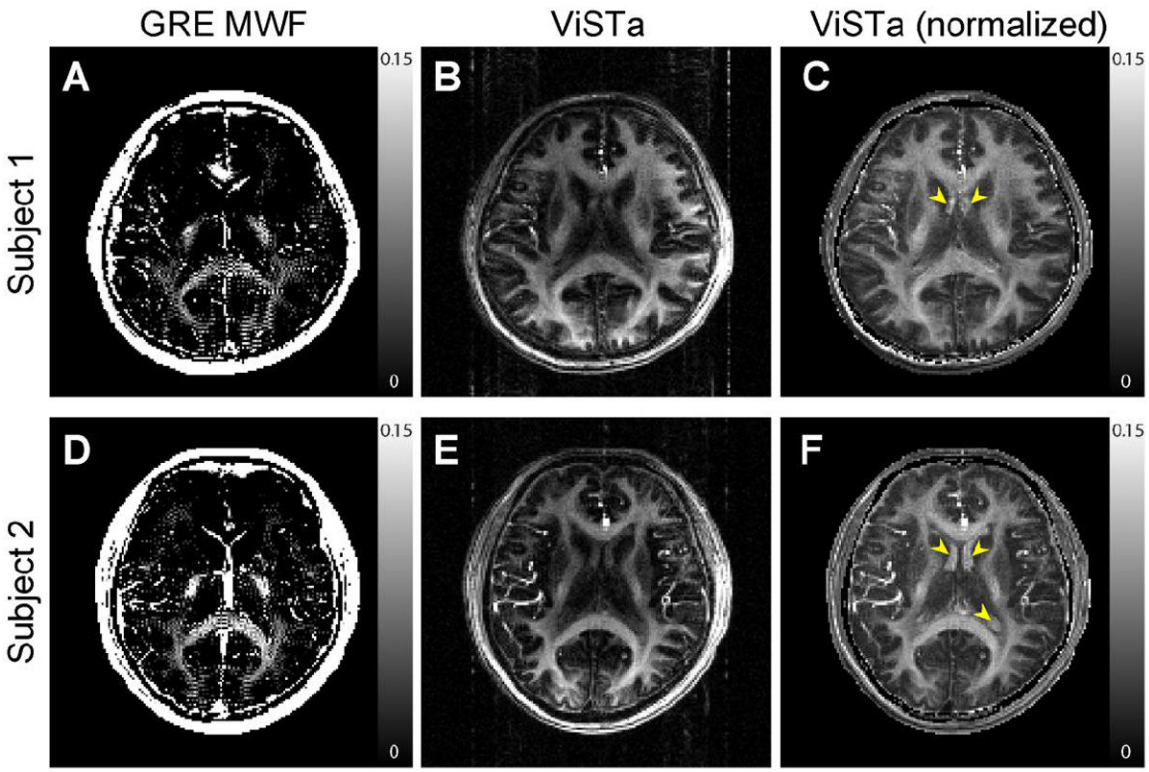

Figure 4.
GRE-MWF (A and D), ViSTa images (B and E), and ViSTa images after normalization (C and F) from two subjects. The ViSTa images (Scan 3 using a single echo with low readout bandwidth) show higher image quality than the GRE-MWF images. Both of them are acquired in 3.1 min. each. Yellow arrows indicate enhanced CSF after normalization.

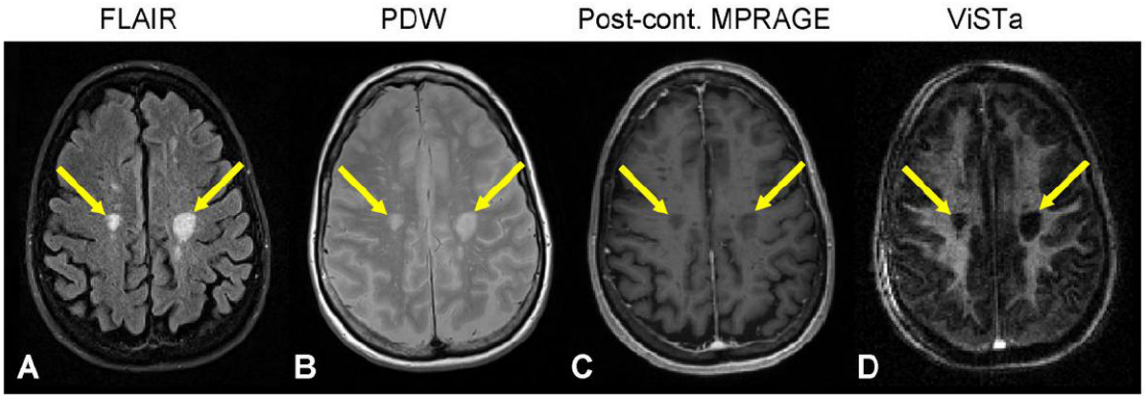

Figure 5.
FLAIR (A), PDW (B), post-contrast MPRAGE (C), and single-echo ViSTa (D) images from an MS patient. Chronic lesions (arrows) show significant signal reduction in the ViSTa image.

Table 1

List of the short T_2^* fractions at ROIs (mean ± standard deviation).

	Fraction of short T_2^* component			
	GRE MWF (Scan 2)		ViSTa (Scan1)	
	Signal averaged in ROI	Pixel-by-pixel estimation	Relative to ViSTa signal	Relative to total water signal
Genu	-	-	(100 ± 0.0%)	5.8 ± 0.4%
Splenium	8.0 ± 0.8 %	8.9 ± 1.8 %	91.4 ± 5.6%	5.4 ± 0.3%
Major forceps	5.8 ± 0.7 %	5.8 ± 0.8%	95.2 ± 3.4%	5.2 ± 0.4%
Minor forceps	-	-	(99.7 ± 0.6%)	5.0 ± 0.4%
Internal capsule	7.7 ± 2.1 %	7.9 ± 2.0 %	99.6 ± 0.4%	5.9 ± 0.2%
Mean	7.2 ± 1.2 %	7.5 ± 1.6 %	95.4 ± 4.1%	5.5 ± 0.4%